

Determination of the calcium ground state scattering length by photoassociation spectroscopy at large detunings

F. Vogt¹, Ch. Grain¹, T. Nazarova¹, U. Sterr¹, F. Riehle¹, Ch. Lisdat^{2,a}, and E. Tiemann²

¹ Physikalisch-Technische Bundesanstalt, Bundesallee 100, 38116 Braunschweig, Germany

² Institut für Quantenoptik, Leibniz Universität Hannover, Welfengarten 1, 30167 Hannover, Germany

Received 28 February 2007

Published online 1st June 2007 – © EDP Sciences, Società Italiana di Fisica, Springer-Verlag 2007

Abstract. Photoassociation spectroscopy was used to determine the s-wave scattering length of ⁴⁰Ca atoms in their electronic ground state. Vibrational levels were observed in an extended range of up to 182 GHz below the dissociation limit $4s^2\ ^1S_0-4s4p\ ^1P_1$. Thus, the frequency interval was nearly tripled, in which photoassociation was observed compared to previous measurements. The spectra were analyzed by means of quantum mechanical simulations. With the new data it was possible to resolve the discrepancy concerning the ground state scattering length presented in earlier publications [Phys. Rev. A **67**, 043408 (2003); Eur. Phys. J. D **26**, 155 (2003)]. An improved dipole-dipole coupling constant $C_3^2 = 0.52306(20) \times 10^3\ \text{cm}^{-1}\ \text{nm}^3$ is obtained.

PACS. 32.80.Pj Optical cooling of atoms; trapping – 34.50.Rk Laser-modified scattering and reactions – 34.10.+x General theories and models of atomic and molecular collisions and interactions (including statistical theories, transition state, stochastic and trajectory models, etc.)

1 Introduction

Photoassociation of ultracold atoms is a well established tool for the production of ultracold molecules and the investigation of cold collision properties [1–3]. Since the association of cold atoms takes place at comparatively large internuclear distances, data from photoassociative spectroscopy contains information on the interaction of two atoms in this region mediated by the molecular potential. Here, the scattering properties of atoms in the ground state as well as the excited molecular state are involved.

Photoassociation of alkaline earth-like atoms was first accomplished with cold calcium [4] and produced lately remarkable results for Sr [5,6] and Yb [7]. It is very interesting to combine and compare the results from photoassociation with complementary experiments like from molecular spectroscopy as it was done for sodium [8] or more recently for potassium [9]. For alkaline earth atoms, only in the case of calcium data from molecular spectroscopy are available for the long range interaction between two atoms [10]. Comparison between the scattering length in reference [10] with data from photoassociation spectroscopy [11] showed a significant deviation.

In this paper we report on new photoassociation measurements that cover an extended energy interval of the B $^1\Sigma_u^+$ state below the asymptote $4s^2\ ^1S_0 + 4s4p\ ^1P_1$ (Sect. 2). The data are modeled with a quantum mechani-

cal formalism described in Section 3 that allows for quantitative description of the experimental results. To precisely reproduce the observations and to determine absolute photoassociation rates, accurate potential curves are necessary for the ground and excited state. Via the adjusted potentials we gain access to the ground state scattering length and the dipole-dipole coupling constant C_3 of the excited state. In Section 4 we discuss the results of the adjustment and give improved values for the lifetime of the atomic level $4s4p\ ^1P_1$ and the ground state s-wave scattering length.

2 Experiment

2.1 Set-up and sequence

We investigate the photoassociation (PA) of cold calcium atoms in a magneto-optical trap (MOT), in which the atomic cloud is cooled on the strong transition $4s^2\ ^1S_0-4s4p\ ^1P_1$ at 423 nm to a temperature of 1.5 mK. In photoassociation, a pair of colliding ground state atoms is resonantly excited by a laser field to a bound molecular state. The spontaneous decay of the molecule produces with significant probability a pair of hot atoms, which is no longer trapped in the MOT. Thus, PA induces additional, frequency dependent trap loss. The signature of this loss is a change of the number of trapped atoms.

^a e-mail: lisdat@iqo.uni-hannover.de

The sensitivity of our experimental set-up to the PA-induced trap loss was significantly improved in comparison to earlier experiments of our group on this subject [4, 11]: the vacuum system has been replaced by a new apparatus, in which the MOT is formed by six independent, pairwise counter-propagating and mutually perpendicular laser beams. The beams have a diameter of 10 mm and power of 1 mW each. The trap is loaded from a slow calcium beam, which is decelerated by a Zeeman slower. The slow atomic beam is collimated and deflected to the trap region by a two-dimensional optical molasses. Additionally, the atomic cloud is illuminated by light from a repumping laser at 672 nm to close a leak to the metastable 1D_2 level. At a pressure of 10^{-9} mbar, the trap lifetime exceeds three seconds. This is one order of magnitude longer than in our earlier experiments and enhances strongly the sensitivity to PA-induced trap losses.

All 423 nm laser beams for cooling Ca are generated by frequency doubling light from a titanium-sapphire laser in an external built-up cavity, which is subsequently frequency shifted and switched by acousto-optical modulators (AOMs). The frequency of the laser is stabilized to a separate calcium reference beam. In total, a power of more than 500 mW is available at 423 nm.

The quadrupole field for the MOT stems from water-cooled coils inside the vacuum system, which enable rapid switching of the field. To achieve a high photoassociation rate it is important to use an atomic cloud of high density. With the new experimental apparatus we have increased the peak density above $6 \times 10^{10} \text{ cm}^{-3}$ by efficiently loading the trap for 600 ms at a low gradient of the magnetic field of 0.23 T/m and then rising the current through the coils for 400 ms until about 1 T/m is reached. The root-mean-square (rms) radius of the calcium cloud amounts to 0.5 mm after the compression. Both density and radius of the calcium cloud were determined by absorption images. At high gradient, the loading rate of the trap is very small. Working continuously at high gradient, the atom number would therefore be only 10% of the number we get with the compression sequence.

During the compressed phase, the atoms are illuminated by light from the PA laser for 1.5 s. Here, we use a second titanium-sapphire laser with frequency doubling and an AOM for switching. The loading of the MOT is turned off by extinguishing the Zeeman slower and deflection-molasses beams. The frequency of the PA light is red-detuned from the $^1S_0 \rightarrow ^1P_1$ cooling transition between $\Delta f = -65$ GHz and $\Delta f = -185$ GHz. The precise value is measured by a wavelength meter with an uncertainty of 1 MHz ($\Delta f < -73$ GHz) or by the observation of a beat note between cooling and PA laser. To calculate detunings Δf from the wavelength measured with the wavelength meter, we made use of the Ca $^1S_0 \rightarrow ^1P_1$ transition frequency of 709 078.382(1) GHz [12].

The PA laser beam has a diameter of 3.8 mm in the trap region. Since the dimension of the trap is much smaller than the diameter of the PA laser beam, the spatial variation of the irradiance over the atomic cloud can be neglected in the analysis. For the first measurements, a

standing wave was used for photoassociation. The intensity variation of the standing wave is included in the simulations to account for the different saturation behaviour in nodes and antinodes. The standing wave was later omitted to simplify the theoretical description. The typical peak irradiance with standing wave ranges between 2.0 W/cm^2 for $v^* = 72$ and 8.0 W/cm^2 ($v^* = 85$). The laser beams for the Zeeman slower and the optical molasses are turned off during the photoassociation phase. This leads to a negligible loading rate of the MOT at high gradient and simplifies the interpretation of the PA spectra.

If the PA laser is resonant with a transition from the collisional continuum to the electronically excited state B $^1\Sigma_u^+$, atoms are bound as excited molecules and are mostly lost from the cold atomic cloud by subsequent radiative decay or state changing collisions. A small fraction is recaptured by the MOT [11]. The atom number is detected by an avalanche photodiode, which monitors the trap fluorescence. The fluorescence signal is recorded at the beginning (yielding F_1) and end (F_2) of the photoassociation phase. The ratio $N = F_2/F_1$ gives the fraction of remaining atoms.

The whole sequence of loading, ramping the gradient up and holding it for 1.5 s is repeated without the light from the photoassociation laser. Accordingly, the ratio $N' = F'_2/F'_1$ is determined that differs from N by the PA-induced losses. From both, we can calculate the relative photoassociation losses L by $L = 1 - N/N'$. The frequency of the PA laser was kept within ± 1 MHz by stabilization on a reference cavity and about forty PA cycles were averaged for each detuning Δf that was investigated.

With the improved trap life time and the increased density, we were able to observe trap loss signals of more than 35%. The strongly increased signal compared to previous investigations (1% trap loss, Ref. [11]) allowed for an increased signal-to-noise ratio and a refined analysis.

Under these improved experimental conditions it was possible to extend the region, in which photoassociation lines were observed, to 182 GHz below the asymptote. Typically, the maximum trap loss was kept below 20% by reducing the PA laser power to avoid saturation of the rotational lines.

The photoassociation spectrum of the vibrational level $v^* = 85$ of the state B $^1\Sigma_u^+$ is depicted in Figure 1 with frequency steps of about 14 MHz. Here, the vibrational quantum number v^* is counted with respect to the asymptote [4, 11], since the absolute assignment is unknown. Our calculations using an approximated potential for the state B give an absolute value for the vibrational assignment of about 177.

2.2 PA-induced loss coefficient

The theoretical model, which we will describe in Section 3, predicts the photoassociation-induced atomic density loss $\dot{\rho} = -\beta\rho^2$ using a loss coefficient β . This coefficient determines together with the background collision rate α the time evolution of the atom number $N(t)$ in the trap, when

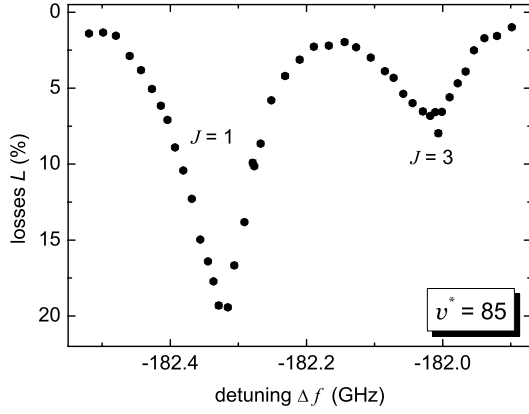


Fig. 1. Photoassociation spectrum of $v^* = 85$ of the state $B \ ^1\Sigma_u^+$ with a sample temperature of 1.5 mK. Transitions to the rotational levels with $J = 1$ and 3 are observed. The detuning Δf is measured with respect to the asymptote $^1S_0 + ^1P_1$.

other many body effects can be neglected:

$$\begin{aligned} \dot{N} &= -\alpha N - \beta \int dr^3 \rho^2(r) \\ &= -\alpha N - \frac{\beta}{8\pi^{3/2}\sigma^3} N^2. \end{aligned} \quad (1)$$

Here, $\rho(r)$ is the local density and σ is the rms trap radius. We have assumed for the trap a Gaussian density distribution and that β is constant over the trap dimension because of the wide photoassociation beam. This equation describes the decay correctly if no loading of the MOT is present, as it is the case in our experiment during the photoassociation phase. The solution of the differential equation (1) is

$$N(t) = N_0 e^{-\alpha t} \left[1 + \frac{N_0 \beta (1 - e^{-\alpha t})}{8\alpha \sigma^3 \pi^{3/2}} \right]^{-1}, \quad (2)$$

with the initial atom number N_0 . Equation (2) can be used to express the relative photoassociation-induced trap loss $L(t)$

$$L(t) = 1 - \left[1 + \frac{\rho_0 \beta (1 - e^{-\alpha t})}{2^{3/2} \alpha} \right]^{-1}, \quad (3)$$

where we made use of the expression for the initial peak density ρ_0

$$\rho_0 = \frac{N_0}{(2\pi)^{3/2} \sigma^3}. \quad (4)$$

With the help of equation (3), one can express β in terms of the experimentally observed trap loss L :

$$\beta = \frac{2^{3/2} \alpha}{\rho_0 (1 - e^{-\alpha t})} \left(\frac{1}{1 - L(t)} - 1 \right). \quad (5)$$

Note, that according to its definition at the beginning of this section β depends neither on the PA time nor on the density. If the trap parameters ρ_0 and α are known,

it is possible to derive the absolute value of β from the experimental results.

The trap lifetime α^{-1} was determined several times during each PA measurement via recording the decrease of the trap fluorescence during hold times (>10 s) at high MOT gradient. It showed a simple exponential decay at all times such that the assumption of negligible two and three body losses is justified (compare Eq. (1) for $\beta = 0$).

The peak density ρ_0 was determined by recording absorption images initially without imaging lens. We assumed cylindrical symmetry of the atomic cloud around the strong vertical axis and σ^3 in equation (4) is replaced by $\sigma_w^2 \sigma_s$ for the weak and strong axis of the MOT, respectively. For high MOT gradient we observed peak densities ρ_0 between $3 \times 10^{10} \text{ cm}^{-3}$ and $9 \times 10^{10} \text{ cm}^{-3}$. Additionally, we took absorption pictures of the released cloud and modeled the expansion using the atomic temperature, which is known from spectroscopy of the Doppler broadened intercombination line $^3P_1 - ^1S_0$ [13]. These measurements showed that the density deduced from earlier absorption images was slightly too small, probably due to a cloud seemingly enlarged by diffraction effects. Modeling the diffraction effects and later adding a lens to image the shadow of the cloud on the CCD camera yielded that though the absolute measured densities are at most a factor of 2 too small, the relative densities are correct within a few percent. Hence, the experimentally determined absolute values of β from equation (5) have a large uncertainty due to the renormalization of the density but relative ones can be compared with theory with high accuracy.

3 Theoretical description

The trap loss signal, which is experimentally observed, depends on three factors: the excitation process, the subsequent decay mechanism including the recapture probability and the response of the trap to the PA-induced losses. The combination of the first two factors leads to the photoassociative loss coefficient β , which was introduced in Section 2.2. The trap response on the PA-induced losses was analyzed in the same section. The aim of this section is the theoretical modeling of β . If β is known for the experimental conditions of laser power and frequency, as well as for a given temperature of the atoms in the trap, the relative losses can be calculated according to equation (3).

To calculate the β parameter, we follow the approach developed by Bohn and Julienne [14] that can be applied very successfully for the description of photoassociation spectra [15]. Using the reflexion approximation, the excitation/stimulated emission rate Γ/\hbar and the light shift E_1 of the transition due to coupling of the photoassociation laser field can be calculated:

$$\Gamma = 2\pi (V_{\text{rad}})^2 \left(\frac{\partial E_b}{\partial v} \right) \frac{|f_0(R_C)|^2}{D_C}, \quad (6)$$

$$E_1 = -\pi (V_{\text{rad}})^2 \left(\frac{\partial E_b}{\partial v} \right) \frac{f_0(R_C) g_0(R_C)}{D_C}. \quad (7)$$

This requires for a given collision energy ϵ the regular (f_0) and irregular (g_0) scattering wave function of ground state atoms at the Condon point R_C . Note the minus sign in equation (7), which corrects a typing error in equation (3.7) in reference [14]. The vibrational spacing in the excited state B $^1\Sigma_u^+$ is expressed by $\partial E_b/\partial v$ at the energy of the molecular level (E_b). The ground state asymptote $^1S_0+^1S_0$ serves as energy reference.

V_{rad} is the radiative coupling between the continuum state and the excited bound molecular level. It incorporates selection rules and relative transition strengths to different rotational levels J from various partial waves ℓ according to the Wigner-Eckart theorem [16] for a transition $\ell, m_\ell \rightarrow J, M$ for polarization q ($q = 0$: π polarization; $q = \pm 1$: σ^\pm polarization):

$$(V_{\text{rad}})^2 = \frac{3\pi c^2 h I}{\tau \omega^3} \frac{1}{4} f_{\text{mol}}(R_C) (2\ell + 1)(2J + 1) \times \begin{pmatrix} \ell & 1 & J \\ m_\ell & q & -M \end{pmatrix}^2 \begin{pmatrix} \ell & 1 & J \\ 0 & 0 & 0 \end{pmatrix}^2. \quad (8)$$

Here, τ is the lifetime of the atomic level $4s4p \ ^1P_1$, ω denotes the angular transition frequency of the 1S_0 to 1P_1 transition, and I is the intensity of the PA laser field. The function $f_{\text{mol}}(R)$ describes retardation effects of the dipole moment and is given in equation (4) of [17]. The zeros in the second $3J$ symbol appear, since we are dealing with a so-called parallel transition between two $^1\Sigma$ states.

Additionally, the derivative of the potential $U(R)$ of the excited state is needed at the Condon point

$$D_C \equiv \left. \frac{\partial U}{\partial R} \right|_{R_C}. \quad (9)$$

The regular and irregular wave functions are determined using the potential curve of the ground state given in reference [10] as starting point. The B state potential curve is represented at large internuclear distance by the atomic pair energy D for $^1S_0+^1P_1$, dispersion coefficients C_3 and C_6 , and the rotational barrier involving the reduced mass μ :

$$U(R) = D - \frac{C_3}{R^3} f_{\text{ret}} - \frac{C_6}{R^6} + \frac{\hbar^2 [J(J+1) + 2]}{2\mu R^2}. \quad (10)$$

f_{ret} denotes the retardation of the resonant dipole-dipole interaction according to e.g. equation (3) in [17]. The inner part of the potential ($R < 0.95$ nm) is replaced by a boundary condition following the idea of the accumulated phase method [18]. The boundary condition and the dipole-dipole coupling constant C_3 can be adjusted to match the observed level structure. The constant C_6 is included to check the sensitivity of the C_3 determination on higher order dispersion coefficients.

We checked the validity of the reflexion approximation, on which the formalism relies, by comparison with calculations involving the full integration over both wave functions. For this purpose, the potential of the state B had to be parametrized over the full range of internuclear

distance, and the inner part was taken from reference [19]. No significant deviation was found. Thus it was possible to use the reflexion approximation to reduce the numerical effort to a level that allows for systematical investigations of different experimental conditions and potentials.

Values of Γ and E_1 were tabulated for the vibrational and rotational levels of interest for a series of collision energies ϵ with $h \times 500$ kHz energy spacing at the respective experimental PA laser intensity. Partial waves ℓ are considered up to $\ell = 6$. Using Γ and E_1 , the excitation probability $|S|^2$ to a given molecular level (v^*, J) can be expressed by

$$|S(\Delta, \epsilon, \ell, v^*, J)|^2 = \frac{1}{2\ell + 1} \sum_{m_\ell} \frac{\hbar \gamma \Gamma(m_\ell)}{[\epsilon - (\Delta + E_1(m_\ell))]^2 + \left(\frac{\hbar \gamma + \Gamma(m_\ell)}{2}\right)^2}. \quad (11)$$

The decay rate γ is determined by the lifetime of the excited molecular level, which is for the long range levels of the state B in good approximation twice the atomic lifetime of the level $4s4p \ ^1P_1$. The detuning $\Delta/h = [\nu(v^*, J) - \nu_L]$ is defined between the molecular level at energy $h\nu(v^*, J)$ and the laser frequency ν_L .

We define a modified trap loss probability S^* , that reflects the probability that a spontaneous decay leads to a trap loss

$$|S^*|^2 = (1 - p)|S|^2. \quad (12)$$

The pre-factor $(1 - p)$ in equation (12) takes into account the probability p that a decay does not lead to a trap loss. Simulations of our MOT show that decay processes that produce atom pairs with a kinetic energy of below 0.7 K lead most likely to a recapture and therefore do not appear as trap loss. The probability of such decay processes can be calculated within the Franck-Condon approximation, which is well justified for the long range part, at which the decay predominantly takes place. The recapture probability p is calculated for each molecular level (v^*, J) summing over outgoing partial waves ℓ . It is in the order of 40% to 25% for v^* considered in this work.

Integrating $|S^*|^2$ over collision energies ϵ assuming a Boltzmann distribution in the trap and summing over ℓ yields the trap loss parameter β

$$\beta(\Delta, v^*, J) = \frac{2}{h Q_T} \sum_{\ell} (2\ell + 1) \int d\epsilon \exp(-\epsilon/k_B T) |S_\ell^*|^2. \quad (13)$$

The factor 2 accounts for the fact that two atoms are lost if one molecule is decaying. The integration is truncated for high energies at values, for which the Boltzmann factor has dropped to 10^{-4} of its maximum value for the experimentally determined atom temperature T . Q_T is the partition function for the atomic temperature T

$$Q_T = \left(\frac{2\pi\mu k T}{h^2} \right)^{3/2}. \quad (14)$$

Knowing our experimental conditions, equations (13) and (3) can be used to quantitatively describe the observed

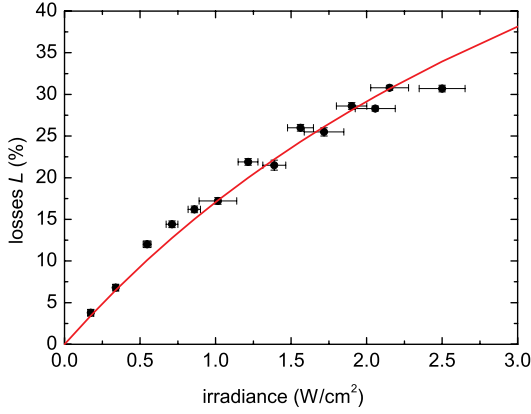


Fig. 2. Saturation behaviour of the photoassociation resonance $v^* = 72$, $J = 1$. The line is a fit according to equation (3) assuming a linear dependence of β on the irradiance.

photoassociation spectra. As we will discuss in Section 4.3, the relative intensity of the rotational lines is very sensitive to the ground state scattering wave function and in particular to the ground state scattering length [20].

4 Results

4.1 Saturation behaviour

To compare the relative intensities of the rotational lines belonging to one vibrational level observed by photoassociation, it is important to avoid saturation of the trap loss and thus leveling of the line intensities. On the other hand, strong signals with good signal-to-noise ratio are preferable for a precise determination of the line intensity.

Since we observe comparatively high atom loss and accordant density reduction, saturation due to the depletion of the trap can be expected [21]. This effect depends on the number of photoassociated molecules and therefore on the PA laser intensity and the photoassociation time. But saturation may also arise from the irradiance dependence of the PA loss coefficient β itself.

To distinguish both processes and to determine a good working point, we have measured relative trap loss L as a function of the PA laser irradiance on the line $v^* = 72$, $J = 1$. The results are shown in Figure 2, saturation is clearly visible. The line depicts a fit of the observed trap loss by equation (3) under the assumption that β is proportional to the irradiance, thus not saturated. Only this proportionality constant was fitted, the other quantities in equation (3) were determined independently.

The good description of the data by the fit shows that the saturation is due to the depletion of atoms from the trap by photoassociative-induced losses. Indications for the saturation of β are not visible. For the experiments described below, the irradiance was chosen such that a trap loss of 25% was not exceeded.

Table 1. Summary of level binding energies E_b in the $B^1\Sigma_u^+$ potential curve determined by the line shape simulations (see text). The corresponding detunings E_b/h from the asymptote are given in GHz. The last column gives the classical outer turning point R_C .

v^*	$J = 1$	$J = 3$	R_C
85	-182.470(10)	-182.115(10)	4.4 nm
80	-126.611(10)	-126.323(10)	5.0 nm
72	-67.087(10)	-67.901(10)	6.2 nm
69	-51.916(10)	-51.777(10)	6.7 nm

4.2 Level structure

The newly observed photoassociative resonances down to -182 GHz below the asymptote $4s^2^1S_0 + 4s4p^1P_1$ allowed for an improved long range description of the state $B^1\Sigma_u^+$. The asymptotic model described in Section 3 was used to fit the observed level energies. Since the classical outer turning point of $v^* = 85$ is located at 4.4 nm only, the potential description (see Eq. (10)) was extended with respect to reference [11] by the van der Waals coefficient C_6 . As energy reference the lowest asymptote $4s^2^1S_0 + 4s^2^1S_0$ was chosen. Hence the atomic pair energy D is given by the transition energy $\hbar\omega$ of the Ca resonance line $^1S_0 - ^1P_1$.

In the determination of the level energies from the photoassociation spectra, special care has to be taken to avoid errors by two effects: most importantly, the thermal averaging (see Eq. (13)) leads to a line shift, which is not negligible at a temperature of the atom cloud of 1.5 mK. Secondly, light shifts as described by equation (7) can be significant.

Both effects can be modeled quantitatively by the formalism described in Section 3. As we will discuss in the next section, a very satisfactory description of the spectra can be achieved. The level energies used to calculate the detuning Δ in equation (11) can be regarded as free of the above mentioned effects. Of course, the analysis invokes the potential of the excited state itself via equations (6) and (7) and the dependence of the rotational structure on the potential. Consequently, the calculations have to be done iteratively, but require a few iterations only to achieve convergence. A list of the determined level energies is given in Table 1.

Since the leading C_3 coefficient originating from the resonant dipole-dipole interaction in the potential description (see Eq. (10)) is connected to the decay rate γ_{at} of the atomic level $4s4p^1P_1$ via the expression

$$\gamma_{at} = \frac{2\omega^3}{3\hbar c^3} C_3, \quad (15)$$

we can give an improved value for γ_{at} . With $C_3/hc = 0.52306(20) \times 10^3 \text{ cm}^{-1} \text{ nm}^3$, one finds $\gamma_{at} = 2.1558(8) \times 10^8 \text{ s}^{-1}$. The uncertainty stems mainly from the correlation with the C_6 coefficient, which was set to $C_6/hc = 32.2 \text{ cm}^{-1} \text{ nm}^6$ and is varied by a factor of 2 to give the error limit above. The fit quality of the observed photoassociation levels is not altered significantly. The uncertainty from the validity of the asymptotic description plays a minor role, which we verified by replacing the

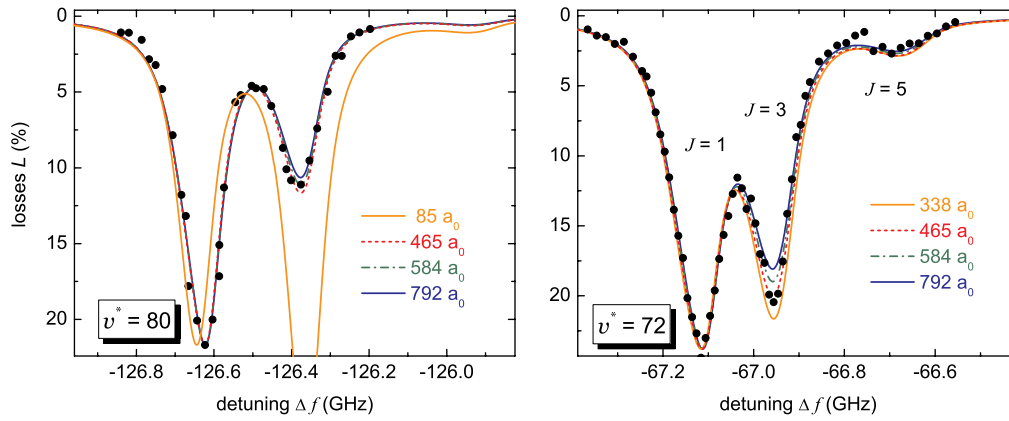


Fig. 3. (Color online) Measured photoassociative spectra of $v^* = 72$ (right hand side) and $v^* = 80$ (left hand side) are depicted by dots. The lines show simulations according to the respective experimental conditions with different ground state s-wave scattering lengths.

nodal line by an approximated short range potential (see Sect. 3) and fitting the repulsive potential branch. The relative variation of C_3 was found to be below 5×10^{-4} . The new value for γ_{at} is in agreement with our previous one ($2.150(19) \times 10^8 \text{ s}^{-1}$ in Ref. [11]) and in remarkable agreement with the theory value of $2.156(30) \times 10^8 \text{ s}^{-1}$ in reference [22], but shows some deviation from recent calculations (Ref. [23], $2.169 \times 10^8 \text{ s}^{-1}$).

4.3 Scattering length

Due to the comparatively high temperature in our experiment, the influence of higher partial waves than the s-wave is of importance. At least g-waves contribute considerably to the spectra, as can be seen by the presence of $J = 5$ resonances in the spectra depicted in Figure 3. The lines show results of simulations using the model described in Section 3 under the respective experimental conditions for selected different ground state scattering lengths. The scattering length was changed by slight variation of the repulsive branch of the ground state potential. As was mentioned before in Section 2, the atomic density had to be adjusted by a factor of about 1.5 to match simulations and experiment. The long range potential of $X^1\Sigma_g^+$ is given by the parameters reported in [10].

As can be seen in Figure 3, the new measurements are well described by the simulations and fit best to a ground state s-wave scattering length in the interval of $340a_0$ to $700a_0$ ($a_0 \approx 0.052918 \text{ nm}$ is the Bohr radius). The sensitivity of the relative line intensity $J = 1/J = 3$ on the scattering length is due to a strong variation of the relative amplitude of s- and d-wave over the internuclear distance, which is probed at different R_C by the vibrational levels in the excited state (see Eqs. (6) and (7)). The range of $R_C = 4.4 \text{ nm} \dots 6.7 \text{ nm}$ is around the maximum of the d-wave rotational barrier at about 5.85 nm .

For these measurements, the temporal stability of the set-up is of great importance, since changes in the trap lifetime, atomic pair density, or PA laser power change the observed trap loss. Hence, in addition to the recordings in Figure 3 several spectra of the discussed lines were quickly recorded with low frequency resolution to be insensitive

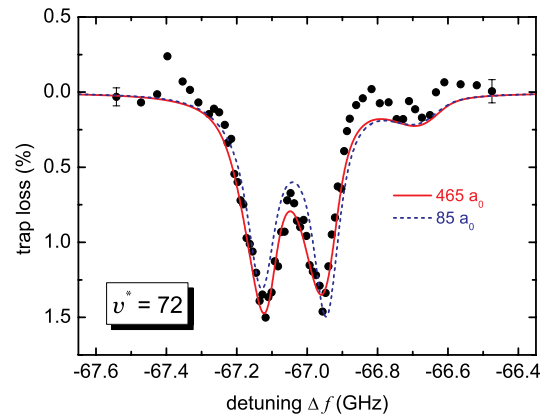


Fig. 4. (Color online) Photoassociation data of $v^* = 72$ from 2003 (dots) [11] together with a simulation according to the model described here (full line) and a s-wave ground state scattering length of $465a_0$. The dashed line is a simulation using a scattering length of $85a_0$. Experimental details are given in [11].

to drifts in the set-up. These measurements confirm the interval of the scattering length given above.

In a previous publication [11] we reported on a determination of the ground state scattering length by similar means but with data up to $v^* = 72$. Then we found a description that favored scattering lengths around $85a_0$. We did not notice the ambiguous description of our previous data by the two scattering lengths $85a_0$ and $465a_0$ due to the lack of data at large detunings and a limited range of investigated scattering lengths. With the new measurements it became apparent that the small scattering length of $85a_0$ cannot describe the whole data set as can be seen in Figure 3. Therefore, a scattering length of $85a_0$ has to be ruled out now. The new analysis is also in much better agreement with data from classical spectroscopy [10], which gives a value between $200a_0$ and $800a_0$. Obviously, the old photoassociation data should be describable with the new potential parameters to give a consistent picture. We have checked this and as example a scan of $v^* = 72$ from 2003 is given together with a new and old ($85a_0$ scattering length) simulation in Figure 4. The description is quite satisfactory.

5 Conclusion

We described new photoassociation experiments at the asymptote $4s^2\ ^1S_0 + 4s4p\ ^1P_1$ of ^{40}Ca . A considerably extended energy interval was covered, which is related to an enlarged range of Condon points in internuclear separation. Therefore, we deduced more accurately the ground state scattering length from our new photoassociation data.

The observations are quantitatively very well described by a model that uses the molecular potentials and experimental conditions to predict the photoassociation spectra. By comparison of simulation and experiment we are able to give an interval for the ground state s-wave scattering length of $340a_0$ to $700a_0$. This is in good agreement with values from classical spectroscopy [10] and resolves the discrepancy to previous PA experiments [11].

With the new data, we are also able to give an improved value of the long range dipole-dipole coupling constant C_3 of the excited state $B\ ^1\Sigma_u^+$, from which we deduce the decay rate $\gamma_{\text{at}} = 2.1558(8) \times 10^8\ \text{s}^{-1}$ for the $4s4p\ ^1P_1$ state of ^{40}Ca .

This work was supported by the German Science Foundation (DFG) within the priority program SPP 1116 and the SFB 407. We thank He Ming for setting up the blue-light system for photoassociation.

References

1. K.M. Jones, E. Tiesinga, P.D. Lett, P.S. Julienne, *Rev. Mod. Phys.* **78**, 483 (2006)
2. J. Weiner, V.S. Bagnato, S. Zilio, P.S. Julienne, *Rev. Mod. Phys.* **71**, 1 (1999)
3. W.C. Stwalley, H. Wang, *J. Mol. Spectrosc.* **195**, 194 (1999)
4. G. Zinner, T. Binnewies, F. Riehle, E. Tiemann, *Phys. Rev. Lett.* **85**, 2292 (2000)
5. M. Yasuda, T. Kishimoto, M. Takamoto, H. Katori, *Phys. Rev. A* **73**, 011403 (2006)
6. T. Zelevinsky et al., *Phys. Rev. Lett.* **96**, 203201 (2006)
7. S. Tojo et al., *Phys. Rev. Lett.* **96**, 153201 (2006)
8. C. Samuelis et al., *Phys. Rev. A* **63**, 012710 (2001)
9. S. Falke, I. Sherstov, E. Tiemann, C. Lisdat, *J. Chem. Phys.* **125**, 224303 (2006)
10. O. Allard et al., *Eur. Phys. J. D* **26**, 155 (2003)
11. C. Degenhardt et al., *Phys. Rev. A* **67**, 043408 (2003)
12. C. Degenhardt, Ph.D. thesis, Universität Hannover, Welfengarten 1, 2004, online available at <http://www.tib.uni-hannover.de>
13. C. Degenhardt et al., *Phys. Rev. A* **72**, 062111 (2005)
14. J.L. Bohn, P.S. Julienne, *Phys. Rev. A* **60**, 414 (1999)
15. C. Lisdat, N. Vanhaecke, D. Comparat, P. Pillet, *Eur. Phys. J. D* **21**, 299 (2002)
16. A.R. Edmonds, *Angular momentum in quantum mechanics* (Princeton University Press, Princeton, New Jersey, 1957)
17. M. Machholm, P.S. Julienne, K.-A. Suominen, *Phys. Rev. A* **64**, 033425 (2001)
18. A. Crubellier et al., *Eur. Phys. J. D* **6**, 211 (1999)
19. O. Allard, Ph.D. thesis, Universität Hannover, Welfengarten 1, 2004, online available at <http://www.tib.uni-hannover.de>
20. E. Tiesinga et al., *J. Res. Natl. Inst. Stand. Technol.* **101**, 505 (1996)
21. R. Wester et al., *Appl. Phys. B* **79**, 993 (2004)
22. S.G. Porsev, M.G. Kozlov, Y.G. Rakhlin, A. Derevianko, *Phys. Rev. A* **64**, 012508 (2001)
23. B. Bussery-Honvault, R. Moszynski, *Mol. Phys.* **104**, 2387 (2006)